Time-resolved measurement of global synchronization in the dust acoustic wave

J. D. Williams*
Department of Physics, Wittenberg University, Springfield, Ohio 45504, USA
(Received 22 August 2014; published 15 October 2014)

A spatially and temporally resolved measurement of the synchronization of the naturally occurring dust acoustic wave to an external drive and the relaxation from the driven wave mode back to the naturally occuring wave mode is presented. This measurement provides a time-resolved measurement of the synchronization of the self-excited dust acoustic wave with an external drive and the return to the self-excited mode. It is observed that the wave synchronizes to the external drive in a distinct time-dependent fashion, while there is an immediate loss of synchronization when the external modulation is discontinued.

DOI: 10.1103/PhysRevE.90.043103 PACS number(s): 52.27.Lw, 52.27.Gr

I. INTRODUCTION

A dusty (complex) plasma is a four-component plasma system that is composed of ions, electrons, neutral particles, and charged microscopic particles or "dust." In the laboratory setting, nanometer- to micrometer-sized particles typically acquire a negative charge through interactions with the background plasma. Once charged, the dust interacts with and self-consistently modifies the properties of the surrounding plasma medium, resulting in a system that is significantly more complex than the traditional three-component plasma and supports a range of new plasma phenomena [1–5], including a collective mode known as the dust acoustic wave [6–11].

The dust acoustic wave is a low-frequency longitudinal mode that propagates through the dust component of the dusty plasma system and is self-excited by the free energy from the ions streaming through the dust component [12]. In the laboratory setting, the majority of the dust acoustic waves that are observed are nonlinear, and, in recent years, there has been a great deal of interest in studying the nonlinear properties of this wave mode [13–26]. Further, the nonlinear nature of the dust acoustic waves that are typically observed in the laboratory facilitates the experimental study of the nonlinear process of synchronization [27–34]. In the context of dusty plasmas, synchronization occurs when the self-excited dust acoustic wave mode couples with and adjusts to an externally applied modulation. In recent years, the fact that this wave mode can synchronize with an external drive has allowed detailed measurements of the properties of this wave mode, including its dispersion relation [35–44].

In this work, we present time-resolved experimental measurements of the global synchronization of the naturally occurring dust acoustic wave to an external drive and the relaxation of the system once the external drive is discontinued by applying a time-resolved Hilbert transform [45] to high-speed imaging of the dust acoustic wave in a dc glow discharge plasma.

II. EXPERIMENTS AND ANALYSIS

The experiment presented here was performed in the Wittenberg University Dusty Plasma Device (Fig. 1) [42]. In this device, an argon plasma is generated by biasing a 2.54 cm (1 in.) in diameter brass electrode positive with respect to the grounded vacuum chamber wall using a voltage controlled constant current power supply at a neutral gas pressure of 90 mTorr.

Dust particles are introduced into the plasma from an electrically floating 2.54-cm-diameter electrode, loaded with 1.98-μm-diameter melamine microspheres (ρ=1510 kg/m^3), positioned approximately 7.5 cm below the anode. Once the plasma has been ignited, these particles acquire a negative charge from the background plasma and are lifted from the tray into the discharge over several minutes to form a stable dust cloud that is observed to be suspended in the anode glow plasma, confined by the gravitational and electrical force due to the self-consistently formed potential structure of the anode. Once the dust cloud has formed, the experimental conditions are adjusted until a self-excited dust acoustic wave is observed to spontaneously appear and propagate in the $-y$ direction, i.e., parallel to the direction of gravity.

For the work that is presented here, the plasma was sustained by biasing the electrode with a voltage of 350 V at a discharge current of 0.35 mA. The plasma parameters ($n_e = 6.7\times10^{16}$ m^{-3}, $T_e = 5.5$ eV) were measured when no dust was present using a double probe. From the images acquired, the average number density of the dust component, $n_{d,o}$, was found to be $n_{d,o} \sim 7.4 \times 10^9$ m^{-3}. Additionally, the normalized wave amplitude $n_d : n_{d,o}$ was measured to be ~1.5–3.5, which provides the nonlinearity necessary for synchronization to occur. The dust charge can be estimated using orbit motion limited (OML) theory [9] and is calculated to be ~6500 electron charges. It is noted that this estimate of the charge is likely larger than the actual dust charge, as OML theory neglects collisional [46] and ionization [47] enhancements to the ion collection that are likely relevant for the experimental conditions here. In particular, it is expected that ionization enhancements to the ion collection will play a more significant role than the collision enhancements given the measured electron temperatures.

To observe the dynamics of this wave mode, the dust particles are illuminated using a 200-mW diode pumped solid state laser ($\lambda = 532$ nm) whose output was expanded into a ~1-mm-thick vertical light sheet and imaged using a Photron SA3 complementary metal-oxide semiconductor camera that is positioned perpendicular to the laser sheet. The camera was equipped with a bandpass filter to eliminate light emitted by

*jwilliams@wittenberg.edu

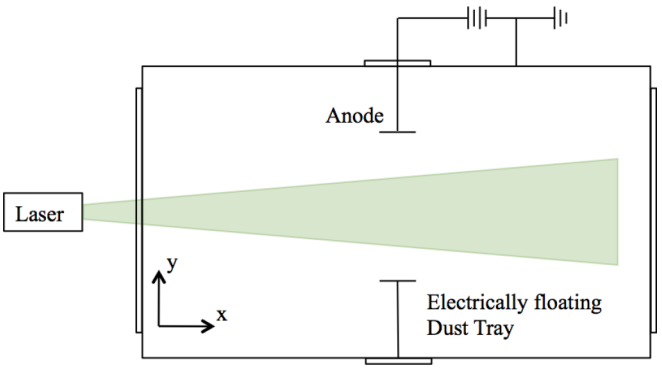

FIG. 1. (Color online) Sketch of the experimental apparatus. The dust clouds examined here formed between the anode and the electrically floating dust tray.

the background plasma glow, and a video sequence consisting of 5000 images was acquired at a rate of 500 fps.

From the image data, the spatiotemporal evolution of the wave mode in the frequency domain was obtained through the use of a time-resolved Hilbert transform. In particular, the mean frequency at a given spatial location was found by constructing the analytic signal from the wave structure by following the general process described previously [20,22,45]. The key steps are detailed below but the reader is referred to [45] for additional details on the application of the time-resolved Hilbert transform.

The wave structure at each pixel location in the acquired images as a function of time, $n_d(x,y,t)$, is found by applying a Gaussian low-pass filter to each image to suppress the effects of the granularity of individual particles and then subtracting the time averaged background dust density, $n_{d,o}$, from each filtered image. The analytic signal, $A(x, y, t)$, is then constructed by expanding the measured wave structure into the complex plane according to Eq. (1):

$$\begin{aligned} A(x,y,t) &= n_d(x,y,t) + \imath \hat{n}_d(x,y,t) \\ &= E(x,y,t)\exp[i\phi(x,y,t)], \end{aligned} \tag{1}$$

where $\hat{n}_d(x,y,t)$ is the Hilbert transform of the measured wave structure, n_d(x, y, t), $E(x, y, t) = (n_d^2 + \hat{n}_d^2)^{1/2}$ is the envelope function, and $\phi(x,y,t) = \text{atan2}[\hat{n}_d(x,y,t), n_d(x,y,t)]$ is the instantaneous phase. The instantaneous phase is then unwrapped to eliminate discontinuities due to phase jumps from 2π to zero. From this, the instantaneous frequency, $f_i(t_o)$, can be found from the derivative of the unwrapped instantaneous phase:

$$f_i(t_o) = \frac{1}{2\pi}\frac{\partial\phi(t)}{\partial t}\bigg|_{t=t_o}. \tag{2}$$

The signal to noise ratio is improved by averaging over several values of the instantaneous frequency, $f_m = \langle f_i(t)\rangle_{\Delta t}$. In this analysis, $\Delta t = 136$ ms (two wave periods at 15 Hz) was used to provide the needed temporal resolution while optimizing the signal to noise ratio.

To examine the synchronization of the naturally occurring dust acoustic wave to an external drive and the relaxation of the system once the external drive is discontinued, a sinusoidal modulation, $I_{\text{mod},pp} = 0.036$ mA, was superimposed on the discharge current, $I_{\text{dis}} = 0.35$ mA, at a frequency of 15 Hz for 4 s (i.e., 60 cycles) beginning 3 s after the camera began acquiring data. An image sequence showing the synchronization and relaxation process are seen in Figs. 2(a) and 2(b) and Figs. 2(c) and 2(d), respectively. Movies showing the spatiotemporal evolution of the wave structure and spatial distribution of the frequencies during these processes can be viewed online (see Ref. [48]).

III. DISCUSSION

The synchronization of the dust acoustic wave with an external drive over the illuminated slice is seen in the time sequence ($\Delta t = 140$ ms) of images depicted in Figs. 2(a) and 2(b). The leftmost image, $t = 3.06$ s, was taken shortly after the external modulation was initiated, and several features are observed that indicate the wave is the naturally occurring mode, including irregular wave fronts, bifurcations in the wave fronts (near $x = 11$, $y = -12$ mm), and the fact that the observed wave structure does not fill the entire illuminated slice of the dust medium (upper left hand corner of the dust cloud). In the frequency domain, one sees a wide range of frequencies being supported across the wave volume and the existence of frequency clusters, which are indicated by the superimposed contours and described in detail elsewhere [45]. The second image in the sequence, $t = 3.2$ s, occurs shortly after the external modulation is observed to modify the behavior of the wave mode. In particular, one begins to observe two characteristic features in the upper ($x \geqslant -10$ mm) region of the cloud that indicate that the wave mode is synchronizing with the external drive: the wave fronts expand to fill the illuminated slice of the dust cloud, and the spacing of the wave fronts becomes regular. In the lower part of the cloud ($x \leqslant -10$ mm), the features previously identified with the natural wave mode are observed. In the frequency domain, it is observed that the upper region of the cloud has locked to the frequency of the external modulation of 15 Hz, while the lower regions of the cloud exhibit the previously described characteristics of the natural wave mode. As time passes, the region of the cloud exhibiting the characteristics that are associated with the driven mode expands, as indicated by the arrow. This sequence of images suggests the existence of a synchronization front that propagates through the dust cloud, behind which one observes the driven wave mode that is synchronized with the external drive.

Once the external modulation is discontinued, a different process is observed as the wave mode returns to the naturally occurring mode. This process is seen in the time sequence ($\Delta t = 105$ ms) of images depicted in Figs. 2(c) and 2(d). In the two leftmost images, $t = 6.87$ and 6.99 s, the wave is initially observed to be synchronized to the external modulation that is superimposed on the discharge current. In the middle frame, $t = 7.12$ s, the wave is clearly returning to the natural mode. In the image data, one observes that the wave fronts are not as regular throughout the cloud volume and that the wave mode no longer fills the illuminated slice. In the frequency domain, one observes the emergence of a range of frequency modes being supported. This is even more clearly seen in the last two plots. Unlike the transition to the driven mode seen in Figs. 2(a) and 2(b), one does not observe a clear "desynchronization"

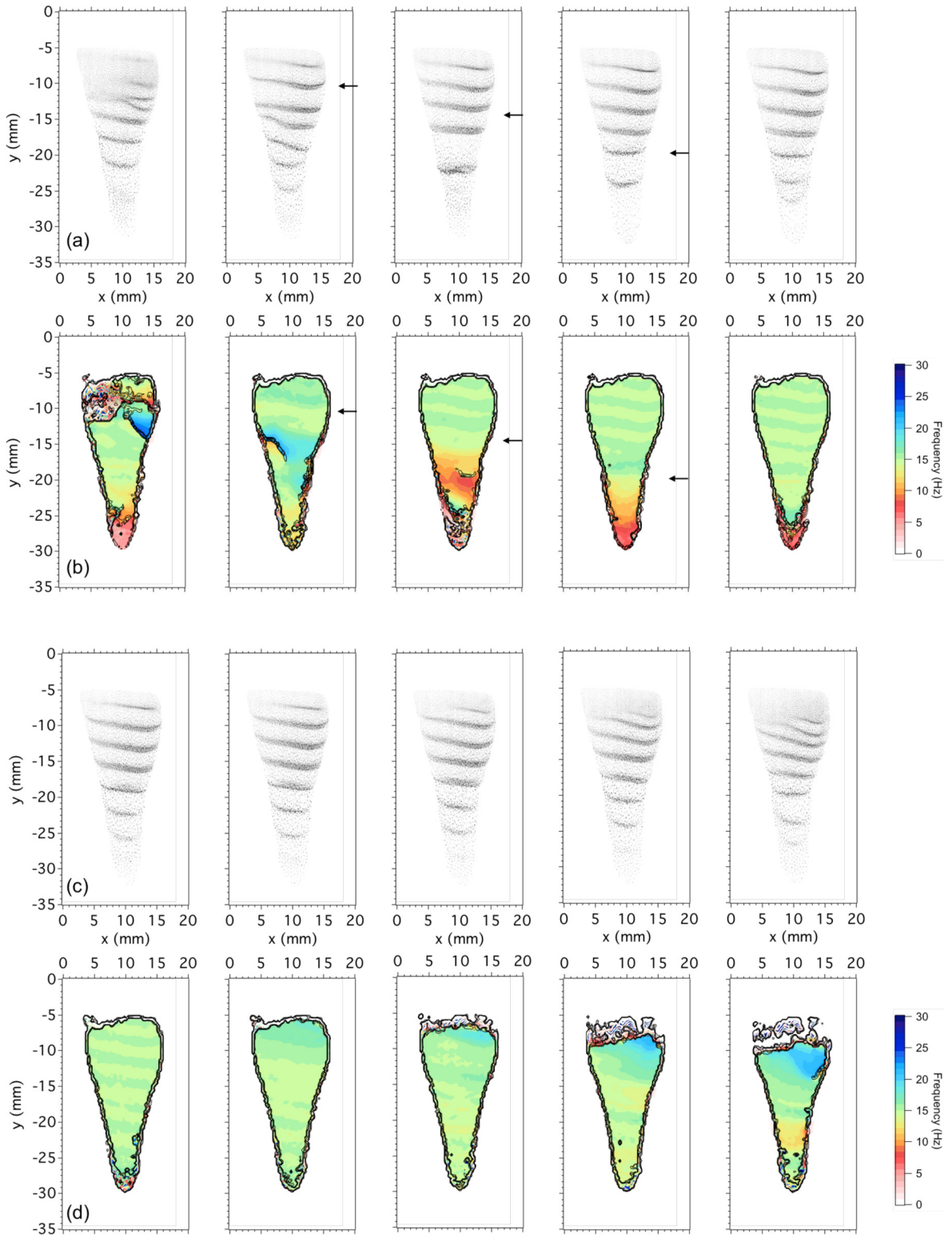

FIG. 2. (Color online) Image sequence showing the temporal evolution of the (a, c) wave and (b, d) spatial distribution frequency (a, b) as the cloud synchronizes with an external drive and (c, d) once the external drive has been discontinued. The spatial distributions of frequency plots have been filtered to only show regions where wave activity is present, and contours depicting where the standard deviation in a 5 × 5 pixel region exceeds 1 Hz have been superimposed to indicate the existence of frequency clusters. The time between images is (a, b) 140 ms and (c, d) 105 ms. Movies showing the time evolution of wave structure and the spatial distribution of frequency as an external drive is initiated and discontinued are available in Ref. [48].

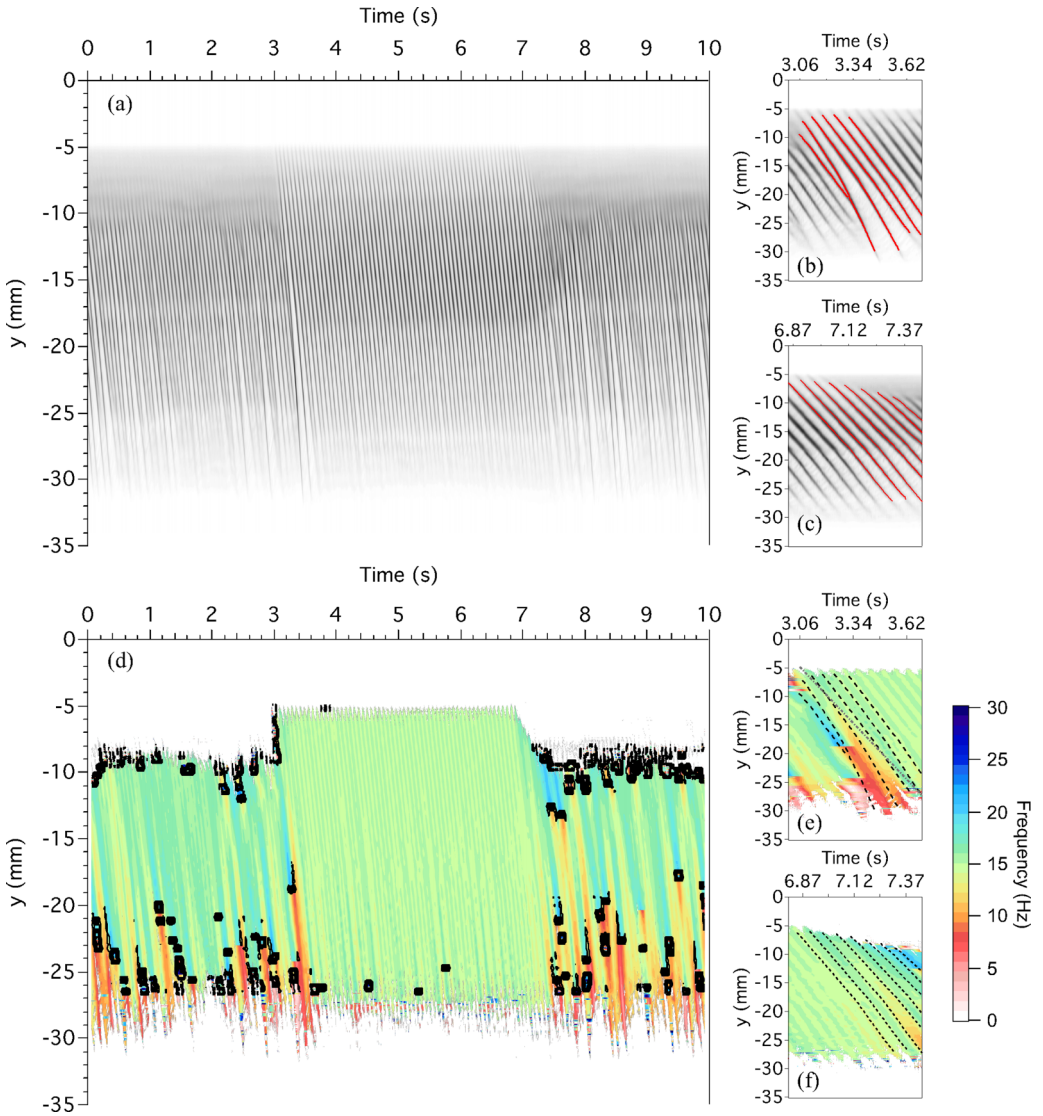

FIG. 3. (Color online) Space-time diagrams constructed from profiles of the (a–c) image intensity and (d–f) spatial distribution of frequencies extracted from $x = 9.87$ mm in Fig. 2. The space-time plots in (d–f) have been filtered to only show regions where wave activity is present, and contours depicting where the standard deviation in a 5×5 pixel region exceeds 1 Hz have been superimposed to indicate the existence of frequency clusters. In (a–c), the dark bands denote the propagation of individual wave fronts through the dust cloud. Expanded views of the synchronization and relaxation process are seen in (b, e) and (c, f), respectively. The superimposed lines (red solid in b, c and black dashed in e, f) depict the propagation of individual wave fronts. The gray dash-dot line in (e) depicts the propagation of a "synchronization" front.

front. Instead, one observes a global relaxation back to the natural mode on a time scale that is notably shorter than is needed to observe synchronization over the illuminated wave volume.

This can also be seen with greater temporal resolution by constructing a space-time plot using a vertical slice at $x = 9.87$ mm from the image and spatial distribution of frequency plots seen in Fig. 2. This is seen in Fig. 3, where each vertical line represents an intensity profile from the imaged dust clouds after applying a Gaussian low-pass filter to each image to suppress the effects of the granularity of individual particles [Fig. 3(a)] and from the frequency data found using the time-resolved Hilbert transform [Fig. 3(d)]. The insets show an expanded view of the synchronization [Figs. 3(b) and 3(c)] and relaxation process [Figs. 3(e) and 3(f)]. The tick marks on the horizontal axes in the insets correspond to the times of the images seen in Fig. 2. Here, one observes the features previously discussed. In particular, two of the previously identified features are particularly evident. First, it is clear here that the synchronization process is not instantaneous, and one can more clearly see evidence of a synchronization front. Additionally, one observes in Fig. 3(e) that this synchronization front (identified by the gray dash-dot line) is not correlated to any of the individual wave fronts (black dashed lines) that are propagating in this vertical slice of the dust cloud and that this synchronization front propagates at a different velocity than the wave fronts. Second, the wave mode relaxes from the driven state almost immediately upon discontinuation of the external modulation and does so in a global fashion without any evidence of the transition front that was observed during transition to the driven mode.

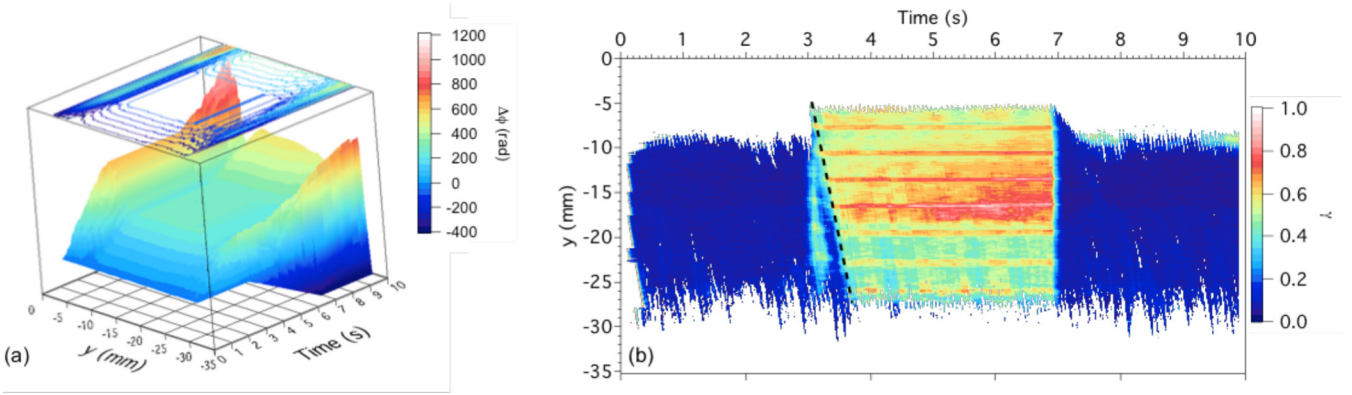

FIG. 4. (Color online) (a) Plot of the cumulative difference in the unwrapped phase between the external modulation and the wave mode at $x = 9.37$ mm. Contours depicting differences in the phase of 50 rad are plotted on the top surface. (b) Space-time-like plot depicting the synchronization index as a function of time at $x = 9.37$ mm. The flat regions that are seen (a) between $t = 3$ and 7 s and the sudden increase in the synchronization index that occurs during this same time provide evidence of synchronization between the external modulation and the dust acoustic wave. The black dashed line depicts the synchronization front identified in Fig. 3(c).

While Figs. 2 and 3 provide strong evidence that the natural wave mode is synchronized to an externally applied drive and illustrate the transition process, more quantitative measures of synchronization between the external modulation and the dust acoustic wave are presented in Fig. 4.

In Fig. 4(a), the cumulative difference in the unwrapped phase $\Delta\phi$, that is found by applying the Hilbert transform to the external modulation $I_{\mathrm{mod},pp}(t)$ and the wave structure at a given location, $n_d(x = 9.37\ \mathrm{mm}, y, t)$ [i.e., $\Delta\phi = \phi_{\mathrm{ext}}(t) - \phi_{\mathrm{wave}}(x = 9.37\ \mathrm{mm}, y, t)$], is plotted. Contours depicting differences in the phase of 50 rad are plotted on the top surface. Using this metric, synchronization is indicated by regions where $\Delta\phi$ remains constant. Here, the flat regions that are seen between $t = 3$ and 7 s provide clear evidence of synchronization between the external modulation and the dust acoustic wave.

A statistical measure of the strength of the synchronization can be found by using a synchronization index [50], $\gamma = \frac{H_{\max} - H}{H_{\max}}$, based on the Shannon entropy [49], $H = \sum_{k=1}^{N} p_k \ln(p_k)$. Here, p_k is the fraction of data in the kth bin in the distribution of the cumulative difference in the unwrapped phase, $\Delta\phi(x = 9.37\ \mathrm{mm}, y, t)(\mathrm{mod} 2\pi)$; $N = 20$ is the number of bins used to construct the distribution of the cumulative difference in the unwrapped phase; and $H_{\max} = \ln(N)$ is the maximum entropy corresponding to a uniform distribution. The distribution of the difference in phases is constructed at each y position at $x = 9.37$ mm using a moving window procedure with 101 consecutive frames centered on time t. This process follows the one recently used by Couëdel *et al.* [51]. This synchronization index scales between zero (desynchronized) and one (fully synchronized), providing a measure of the degree of synchronization. Further, synchronization is indicated by plateaus of elevated values of the synchronization index, γ. A space-time-like plot depicting the synchronization index as a function of y position and time at $x = 9.37$ mm is seen in Fig. 4(b).

From the space-time-like plot depicting the synchronization index [Fig. 4(b)], there are three observations to note about the synchronization process. First, a sudden increase in the synchronization index is seen throughout the cloud when the external modulation is initiated at $t = 3$ s, suggesting that the wave may respond immediately to the external modulation. A closer examination of the space-time plot depicting the spatial distribution of frequency [Fig. 3(d)] shows that the dominant frequency at $x = 9.37$ mm does jump briefly to 15 Hz at $t = 3$ s. However, it is clear from the movie depicting the synchronization process, seen in Ref. [48], that this is not a global response, as some regions of the cloud are observed to be at very different frequencies. This, coupled with the lack of a plateau in the synchronization index, γ, suggests that, while the wave may exhibit an immediate response to the external modulation, the wave does not immediately synchronize with the external modulation. The synchronization index, however, does increase suddenly a short time later and remain at a relatively constant value once the previously identified synchronization front, depicted by the dashed black line, passes through the background dust medium. This, in combination with the previously presented results, suggests that it takes some time for information about the externally applied modulation to reach a location in the dust cloud and for the wave mode to synchronize with the externally applied modulation. This is seen by the existence of a synchronization front whose passing precedes the wave mode synchronizing with the external modulation. Second, once the wave mode has become synchronous with the external modulation, the degree of synchronization is not constant over the wave field. Instead, one observes that the synchronization index initially increases as one moves away from the source of the external modulation before reaching a maximum about halfway through the cloud and then decreases. This is similar to what is seen with the amplitude of the wave, which emerges from the background dust medium at the top of the cloud, grows until a larger amplitude is not supported by the background dust medium, and then decreases as the wave travels toward the bottom of the cloud and dissipates. One also observes that the degree of synchronization increases over time, particularly in the middle region of the cloud. This too is consistent with observations of the wave amplitude in

the middle region of the cloud, where a slight increase in the wave amplitude is observed during the period when the external modulation is applied. This suggests the degree of synchronization may depend on the degree of nonlinearity in the wave. Finally, one observes that when the modulation is discontinued at $t = 7$ s the synchronization index suddenly drops across the entire cloud. This suggests that there is a global and immediate response in the wave mode when the external modulation is discontinued. In particular, there is an immediate loss of synchronization, which is then followed by a more gradual return to the natural wave mode. The different behavior that is observed during the synchronization and relaxation process suggests that there may be different mechanisms responsible for these processes.

IV. CONCLUSION

To summarize, we present time-resolved measurements of global synchronization of the naturally occurring dust acoustic wave with an externally applied modulation and the relaxation process to the natural mode when the external modulation is discontinued. It was observed that it takes some time for the wave mode to synchronize with this external drive. Further, it appears that this synchronization happens behind a propagating synchronization front that travels at a different speed than the phase velocity of the wave mode. When the modulation is discontinued, there is an immediate loss of synchronization, followed by a return to the natural wave mode on a time scale that is shorter than what is observed during the synchronization process.

ACKNOWLEDGMENTS

This work is supported by the US National Science Foundation through Grant No. PHY-0953595. We would like to thank Professor Edward Thomas, Jr. for helpful discussions during the preparation of this manuscript.

[1] N. D'Angelo, Planet. Space Sci. **38**, 1143 (1990).
[2] P. K. Shukla, Plasma Phys. Control. Fusion **42**, B213 (2000).
[3] M. Rosenberg, Astrophys. Space Sci. **277**, 125 (2001).
[4] P. K. Shukla and B. Eliasson, Rev. Mod. Phys. **81**, 25 (2009).
[5] E. Thomas, Jr., Contr. Plasma Phys. **49**, 316 (2009).
[6] N. N. Rao, P. K. Shukla, and M. Y. Yu, Planet. Space Sci. **38**, 543 (1990).
[7] A. Barkan, R. L. Merlino, and N. D'Angelo, Phys. Plasmas **2**, 3563 (1995).
[8] F. Verheest, *Waves in Dusty Space Plasmas* (Kluwer, Dordrecht, 2000).
[9] P. K. Shukla and A. A. Mamun, *Introduction to Dusty Plasma Physics* (Institute of Physics, Bristol, England, 2002).
[10] S. V. Vladimirov, K. Ostrikov, and A. A. Samarian, *Physics and Applications of Complex Plasmas* (Imperial College, London, 2005).
[11] A. Piel, *Plasma Physics: An Introduction to Laboratory, Space, and Fusion Plasmas* (Springer-Verlag, Berlin, 2010).
[12] R. L. Merlino, Phys. Plasmas **16**, 124501 (2009).
[13] J. Pramanik, B. M. Veeresha, G. Prasad, A. Sen, and P. K. Kaw, Phys. Lett. A **312**, 84 (2003).
[14] E. Thomas, Jr., Phys. Plasmas **13**, 042107 (2006).
[15] C.-T. Liao, L.-W. Teng, C.-Y. Tsai, C.-W. Io, and L. I, Phys. Rev. Lett. **100**, 185004 (2008).
[16] V. Nosenko, S. K. Zhdanov, S. H. Kim, J. Heinrich, R. L. Merlino, and G. E. Morfill, Europhys. Letters **88**, 65001 (2009).
[17] L.-W. Teng, M.-C. Chang, Y.-P. Tseng, and L. I, Phys. Rev. Lett. **103**, 245005 (2009).
[18] J. Heinrich, S.-H. Kim, and R. L. Merlino, Phys. Rev. Lett. **103**, 115002 (2009).
[19] T. M. Flanagan and J. Goree, Phys. Plasmas **17**, 123702 (2010).
[20] K. O. Menzel, O. Arp, and A. Piel, Phys. Rev. Lett. **104**, 235002 (2010).
[21] T. M. Flanagan and J. Goree, Phys. Plasmas **18**, 013705 (2011).
[22] K. O. Menzel, O. Arp, and A. Piel, Phys. Rev. E **83**, 016402 (2011).
[23] K. O. Menzel, O. Arp, and A. Piel, Phys. Rev. E **84**, 016405 (2011).
[24] R. L. Merlino, J. R. Heinrich, S. H. Hyun, and J. K. Meyer, Phys. Plasmas **19**, 057301 (2012).
[25] Y.-Y. Tsai, M.-C. Chang, and L. I, Phys. Rev. E **86**, 045402(R) (2012).
[26] J. D. Williams, IEEE Trans. Plasma Sci. **41**, 788 (2013).
[27] B. E. Keen and W. H. W. Fletcher, Phys. Rev. Lett. **23**, 760 (1969).
[28] H. Amemiya, Plasma Phys. **25**, 735 (1983).
[29] T. Klinger, A. Piel, F. Seddighi, and C. Wilke, Phys. Lett. A **182**, 312 (1993).
[30] D. Block, A. Piel, C. Schröder, and T. Klinger, Phys. Rev. E **63**, 056401 (2001).
[31] M. E. Koepke, M. J. Alport, T. E. Sheridan, W. E. Amatucci, and J. J. Carroll, III, Geophys. Res. Lett. **21**, 1011 (1994).
[32] T. Klinger, F. Greiner, A. Rohde, A. Piel, and M. E. Koepke, Phys. Rev. E **52**, 4316 (1995).
[33] O. Fukumasa and R. Itatani, Plasma Phys. **24**, 1503 (1982).
[34] T. Fukuyama, R. Kozakov, H. Testrich, and C. Wilke, Phys. Rev. Lett. **96**, 024101 (2006).
[35] C. Thompson, A. Barkan, N. D'Angelo and R. L. Merlino, Phys. Plasmas **4**, 2331 (1997).
[36] T. Trottenberg, D. Block, and A. Piel, Phys. Plasmas **13**, 042105 (2006).
[37] E. Thomas, Jr., R. Fisher, and R. L. Merlino, Phys. Plasmas **14**, 123701 (2007).
[38] J. D. Williams, E. Thomas, Jr., and L. Marcus, Phys. Plasmas **15**, 043704 (2008).
[39] M. Schwabe, S. K. Zhdanov, H. M. Thomas, A. V. Ivlev, M. Rubin-Zuzic, G. E. Morfill, V. I. Molotkov, A. M. Lipaev, V. E. Fortov, and T. Reiter, New J. Phys. **10**, 033037 (2008).

[40] I. Pilch, T. Reichstein, and A. Piel, Phys. Plasmas **16**, 123709 (2009).
[41] E. Thomas, Jr., Phys. Plasmas **17**, 043701 (2010).
[42] J. D. Williams and E. Snipes, IEEE Trans. Plasma Sci. **38**, 847 (2010).
[43] J. D. Williams and J. Duff, Phys. Plasmas **17**, 033702 (2010).
[44] W. D. Suranga Ruhunusiri and J. Goree, Phys. Rev. E **85**, 046401 (2012).
[45] J. D. Williams, Phys. Rev. E **89**, 023105 (2014).
[46] M. Lampe, R. Goswami, Z. Sternovsky, S. Robertson, V. Gavrishchaka, G. Ganguli, and G. Joyce, Phys. Plasmas **10**, 1500 (2003).
[47] S. A. Khrapak and G. E. Morfill, Phys. Plasmas **19**, 024510 (2012).
[48] See Supplemental Material at http://link.aps.org/supplemental/10.1103/PhysRevE.90.043103 for a movie showing the time evolution of the wave structure and spatial distribution of frequency as an external drive is initiated and discontinued.
[49] C. E. Shannon, The Bell System Technical J. **27**, 379 (1948).
[50] P. Tass, M. G. Rosenblum, J. Weule, J. Kurths, A. Pikovsky, J. Volkmann, A. Schnitzler, and H. J. Freund, Phys. Rev. Lett. **81**, 3291 (1998).
[51] L. Couëdel, S. Zhdanov, V. Nosenko, A. V. Ivlev, H. M. Thomas, and G. E. Morfill, Phys. Rev. E **89**, 053108 (2014).